

Novel Kuramoto model with inhibition dynamics modeling scale-free avalanches and synchronization in neuronal cultures

D. Lucente^{1,*}, L. Cerutti^{2,3,*}, M. Brofiga^{2,3}, A. Sarracino⁴, G.

Parodi², S. Martinoia^{2,5,6}, P. Massobrio^{2,7,‡,†} and L. de Arcangelis^{1,†‡}

¹ *Department of Mathematics & Physics - University of Campania "Luigi Vanvitelli" - Caserta, Italy*

² *Department of Informatics, Bioengineering, Robotics,*

and Systems Engineering (DIBRIS), University of Genova, Genova, Italy

³ *Neurofacility, Istituto Italiano di Tecnologia (IIT), 16100 Genova, Italy*

⁴ *Department of Engineering - University of Campania "Luigi Vanvitelli" - Aversa, Italy*

⁵ *RCCS Ospedale Policlinico San Martino, Largo Rosanna Benzi 10, 16132, Genova, Italy*

⁶ *Inter-University Center for the Promotion of the 3Rs Principles in Teaching & Research (Centro 3R), Genova, Italy*

⁷ *National Institute for Nuclear Physics (INFN), Genova, Italy*

(Dated: December 22, 2025)

Neuronal cultures exhibit a complex activity, bursts, or avalanches, characterized by the coexistence of scale invariance and synchronization, quite stable with the percentage of inhibitory neurons. While this bistable behavior has been already observed in the past, the characterization of the statistical properties of avalanche activity and their temporal organization is still lacking, as well as a model able to reproduce these dynamics. Here, we analyze experimental data of human neuronal cultures with controlled percentage of inhibitory neurons and characterize their statistical properties and dynamical organization. In order to model the experimental data, we propose a novel version of the Kuramoto model for two populations of oscillators, excitatory and inhibitory, implementing successfully the inhibition dynamics. The model can fully reproduce the experimental results, confirming the existence of correlations in the temporal organization of avalanche activity and the presence of an amplification - attenuation regime, as found in the human brain.

I. INTRODUCTION

Neuronal networks, both in vivo and in vitro, often exhibit complex activity patterns characterized by intermittent bursts of activity, named avalanches, separated by periods of relative quiescence. Previous studies on cortical murine cultures have shown that such systems may exhibit neuronal avalanches, with a broad range of sizes and durations, typically following power-law distributions [1, 2]. This dynamical regime has been proposed as a hallmark of criticality, suggesting that the brain might operate near a critical point to optimize information processing [3]. In parallel, in vitro networks also revealed strong synchronization phenomena [4]. The coexistence of distinct dynamical regimes, i.e. quiescent/weakly active states and strongly synchronized states, can be explained by the concept of *self-organized bistability* [5]. Within this framework, criticality and synchronization in excitable networks coexist [6, 7]. A minimal model capturing these features is the active rotator model [7, 8], an extension of the Kuramoto model, which has long been a cornerstone to describe synchronization phenomena and collective dynamics [9, 10]. Unfortunately, the original Kuramoto model is not suitable for reproducing avalanche-like or intermittent dynamics [7]. Conversely, oscillators in the active rotator model exhibit excitable

behavior [11–13], leading the system activity to organize into avalanches whose size and duration distributions exhibit bimodality, consisting of a power-law regime followed by a bump associated with synchronized bursting [7, 14]. More recently, this model has been also extended to analyze synchronization on fruitfly and human connectomes [8, 15].

In this work, we extend the model to include an inhibitory population. Two-population Kuramoto models have been studied extensively in the context of coupled oscillators [16–19], but inhibition is often modeled by simply changing the sign of the interaction constant, which only partially reflects biological interaction since it might enhance the overall activity of the network [19, 20]. Here, instead, the inhibition is taken into account by introducing a time-dependence in the amplitude of the potential term entering the oscillator dynamics, ensuring that the interaction between the two populations leads to biologically plausible inhibition dynamics. Building on this biologically grounded Kuramoto model, we then directly compare experimental and numerical avalanche dynamics obtained from human induced pluripotent stem cells (hiPSCs)-derived cortical networks coupled to Micro-Electrode Arrays (MEAs). These cultures are systematically plated controlling the ratio between excitatory and inhibitory cells to explore how the excitation–inhibition (E:I) balance shapes network activity [21]. In particular, we consider two E:I ratios: the physiological condition with 75% excitatory to 25% inhibitory neurons (75E:25I) and the limit case of fully excitatory networks (100E). It was recently proved that acting on the E:I balance, a modulation of the

* These authors have contributed equally to this study.

† These authors jointly supervised the study.

‡ Correspondence: Paolo.Massobrio@unige.it

lucilla.dearcangelis@unicampania.it

bursting activity is possible: *in vitro* physiological cortical networks display a bursting-dominated activity, purely inhibitory networks abolish bursting activity, while purely excitatory assemblies display only few bursts [21].

Traditional analyses of neuronal avalanches have mainly focused on static properties, such as size and duration distributions and their scaling relations [1]. While informative, these measures do not fully capture the temporal organization of activity. To address this, we complement them with dynamical metrics, including inter-event interval distributions and conditional probabilities linking avalanche sizes to preceding inter-event times [22, 23]. This approach provides deeper insights into the network activity and reveals different dynamical regimes.

The structure of the paper is as follows. Sec. II describes both the experiments and the model, including plating procedures, electrophysiological recordings, and the definition of avalanches. We also present the active Kuramoto model with our novel implementation of inhibition dynamics. Sec. III is devoted to the core analysis of the present work, that is the comparison between experimental and numerical results, examining both static and temporal properties of avalanche activity. We first extract size and duration distributions, showing also the verification of the scaling relation for the conditional expectation of the avalanche size given its duration, predicted by Sethna scaling theory [24–26]. Next, we discuss the properties of the inter-time distributions and explain how we define the physical time-scale of the model through a comparison to the experimental data. We then analyze conditional probabilities of the increments between subsequent avalanches as a function of the time elapsed between them. Finally, we discuss the implications of our findings in Sec. IV.

II. MATERIALS AND METHODS

A. Generation and culturing of hiPSC-derived neuronal networks

Human induced pluripotent stem cells (hiPSCs) have been differentiated in excitatory and inhibitory neurons as described in [21]. Two different excitatory/inhibitory (E:I) configurations have been considered in this work: 100% excitatory (100E) and 75% excitatory / 25% inhibitory (75E:25I). Fig. 1 (A-C) shows representative networks imaging for these two configurations. Electrophysiological recordings have been conducted at 70 days *in vitro* (DIV) by using micro-electrode arrays (MEAs) with 60 TiN electrodes (30 μm diameter, 200 μm spacing, 8×8 grid), connected to the MEA2100 system (Multi Channel Systems, Reutlingen, Germany). After a 10-minute acclimation outside the incubator, spontaneous neuronal activity has been recorded for 15 minutes at 37 °C and sampled at 10 kHz. Data have been pre-processed by

means of the peak detection algorithm devised in [27]. Practically, by setting a differential threshold for each electrode, (8 times the standard deviation of the signal’s biological and thermal noise), the peak lifetime period (1 ms), and the refractory period (0 ms), spikes have been identified and used as peak trains for all the presented analyses.

B. Experimental analysis

The dataset used for the analysis presented in this work consists of $n_{100E} = 6$ and $n_{75E:25I} = 5$ samples for purely excitatory (100E) and physiological (75E:25I) networks, respectively. After spike detection, we estimate the inter-spike interval (ISI) – defined as the time between consecutive spikes in the network. To exclude coincidental simultaneous events, only ISIs greater than 1 ms have been considered. Given the electrode spacing, this threshold ensured that only spikes with a plausible causal relationship have been included in the analysis. The time-bin t_b has been defined as the average ISI. Tab. I reports the values of t_b for 100E and 75E:25I networks.

	100E	75E:25I
Sample	t_b (ms)	t_b (ms)
1	8	12
2	11	6
3	10	11
4	9	8
5	5	9
6	4	–

TABLE I. Time-bin t_b of individual samples for the experiments on purely excitatory (100E) and physiological (75E:25I) configurations.

C. Avalanche detection

To identify avalanches, neuronal activity from each MEA has been organized into raster plots (see Figs. 1 D), where rows correspond to recording channels and columns to recording times. To construct the binned raster plot, the total recording time has been divided into contiguous, non-overlapping time windows (bins) of fixed duration t_b , whose values are reported in (Tab. I), ensuring that the temporal resolution matches the intrinsic timescale of the network. For each channel and bin, the number of detected spikes has been counted. Bins containing at least one spike have been marked as active, while those with no spikes have been marked as inactive. This binarized representation captures the temporal structure of network activity. The overall activity at each time bin has then been obtained as the sum of active channels, and avalanches have been defined as sequences of consecutive active bins, bounded before and after by

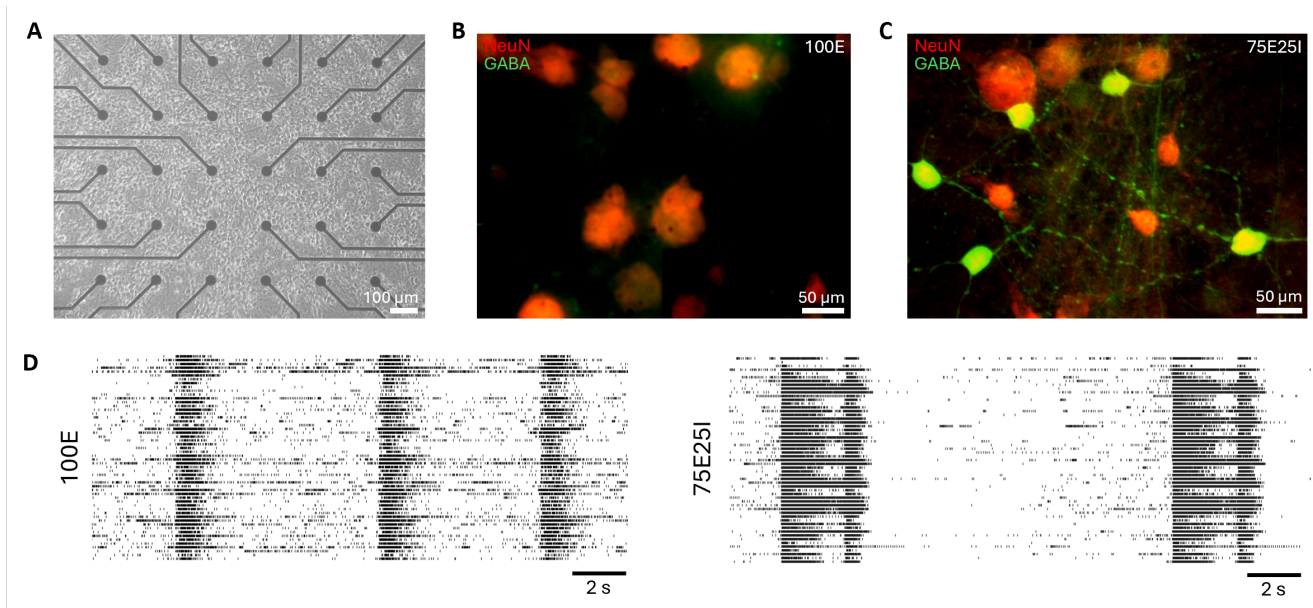


FIG. 1. Representative images of hiPSC-derived neuronal cultures. A) Neuronal network plated on a micro-electrode array (MEA) at a density of 1200 cells/mm^2 ; electrodes are visible beneath the neuronal layer. B-C) Representative network images at DIV70 of (B) 100E and (C) 75E25I cultures. Neurons were labelled for NeuN (red) and GABA (green) to visualize the neuronal population and distinguish GABAergic from glutamatergic populations. D) Raster plots of the spontaneous activity of representative 100E (on the left) and 75E25I (on the right) neuronal cultures at DIV70. A black dot and a dense band represent a detected spike and a network burst, respectively.

at least one inactive bin. Each avalanche is characterized by its size S representing the total number of active electrodes, and its duration T corresponding to the number of consecutive active bins multiplied by the bin size. Finally, the inter-event time Δt has been defined as the time interval between the end of one avalanche and the start of the next one.

D. Avalanche Statistics

The distributions of sizes S and durations T follow power-law distributions[1–3]

$$P(S) \sim S^{-\tau}, \quad P(T) \sim T^{-\alpha}. \quad (1)$$

Within the scale-free regime we also have considered the average size of avalanches with fixed duration T which also follows a power-law dependence on T [24–26]

$$\langle S \rangle_{S|T} \sim T^\gamma. \quad (2)$$

These power-law distributions appear frequently during analysis of experimental data and might not be related to the presence of a critical point [28–30]. Notwithstanding, as demonstrated by Sethna in the context of crackling noise [24–26], for critical systems the exponent γ is related to α and τ by the scaling relation

$$\gamma = \frac{\alpha - 1}{\tau - 1}. \quad (3)$$

The above relation was proven to hold for a wide class of experimental systems or computational models, independently of the values assumed by the two exponents τ and α [31].

E. Inter-time distribution

The inter-time Δt is the duration of the quiescent period that separates the end of a neuronal avalanche and the beginning of the subsequent one. The probability distribution of the inter-times $P(\Delta t)$ differs from the Poisson distribution when avalanches are correlated in time [32]. In this situation, $P(\Delta t)$ might show power-law regimes $P(\Delta t) \sim \Delta t^{-\mu}$ being μ the relative exponent [23].

F. Conditional Probability Analysis

The organization of avalanches of different size in time is evidenced by the study of the conditional probability $P(s_0, t_0)$ of a size difference $\Delta S = S^{(i+1)} - S^{(i)} \leq s_0$ given the value of the inter-time $\Delta t \leq t_0$. Specifically, $P(s_0, t_0)$ is defined as

$$P(s_0, t_0) = \frac{N(\Delta s < s_0; \Delta t < t_0)}{N(\Delta t < t_0)} \quad (4)$$

where $N(\Delta t < t_0)$ is the number of event couples with temporal distance Δt less than t_0 while $N(\Delta s < s_0; \Delta t <$

t_0) is the number of such couples with difference Δs smaller than s_0 . To quantify the strength of correlations, $P(s_0, t_0)$ is compared with a surrogate probability $\bar{P}(s_0, t_0)$ defined as in Eq. (4) but for a different sequence of $\{\Delta S, \Delta t\}$. The surrogate sequence $\{\bar{\Delta S}, \Delta t\}$ is obtained by reshuffling the original avalanche sizes S while preserving the exact occurrence times. This ensures that the marginal distributions of sizes and inter-times coincides with the original ones, but all correlations are destroyed. For a large number of reshuffling \bar{P} is a Gaussian with standard deviation σ . The difference

$$\delta P = P - \bar{P} \quad (5)$$

quantifies the deviation of the real avalanche sequence from random occurrence. If $\delta P \leq 2\sigma$, the real avalanche sequence can be considered as a possible realization of random sequences and, therefore, avalanche sizes and occurrence times are uncorrelated. For fixed t_0 , the behavior of δP as a function of s_0 provides useful information about amplification or attenuation mechanism in avalanche occurrence. A maximum of δP for $\Delta S < 0$ and $\Delta S > 0$, indicates that, on average, avalanches close in time are attenuated or amplified in size, respectively [22, 33].

G. Model

1. Purely excitatory active Kuramoto model

The active Kuramoto model extends the classic one by incorporating conservative forces into the dynamics of coupled oscillators [11, 12, 16, 34–36]. In the standard paradigm, neurons (oscillators) are characterized by their natural frequencies and coupled to all others through phase interactions. A neuron is assumed to fire whenever its phase crosses a fixed threshold (e.g. $\frac{\pi}{2}$). The active model modifies this picture by introducing a conservative force that confines the dynamics of each oscillator close to a stable-fixed point representing the neuron resting potential. In this setting, neurons fire either when random fluctuations push them out of the stability region, or when they are triggered by interactions with connected firing neurons [7, 8]. Formally, each neuron j is represented by a variable θ_j that evolves according to [7, 11, 12, 16]

$$\dot{\theta}_j = \omega_j + \xi_j - \frac{K}{N} \sum_l \sin(\theta_j - \theta_l) + a \sin(\theta_j) \quad (6)$$

where N is the number of coupled oscillators, ω_j is an intrinsic random frequency with distribution $g(\omega)$, K is the coupling strength, a is the amplitude of the conservative force, and ξ_j a Gaussian white noise with variance σ_ξ^2 . The original Kuramoto model corresponds to Eq. (6) with $a = 0$. For $g(\omega) = \delta(\omega - \bar{\omega})$, with $\bar{\omega}$ a fix value of ω , the system can settle close to a critical point where the

oscillators are synchronized and avalanches follow power-law distributions [7, 8]. The critical point corresponds to a particular synchronization transition [7, 8]. Here, we consider $g(\omega) = \mathcal{N}(\bar{\omega}, \sigma_\omega)$, i.e. a Gaussian distribution with standard deviation $\sigma_\omega = 0.1$ and mean $\bar{\omega}$. For the parameters of the model, unless otherwise specified, we set $K = 1$, $\bar{\omega} = 1$, $a = 1.055$, $\sigma_\xi = 0.42$, and $N = 500$.

To perform the analysis of numerical avalanche dynamics, we must first define how spikes are extracted from oscillator phases and how the corresponding raster plot is built. Following [7], we associated to each neuron with phase θ_j a function

$$y_j = 1 + \sin(\theta_j) \quad (7)$$

which spans from 0 to 2 for $\theta_j \in (-\pi, \pi]$. Spikes of j -th neuron are identified whenever y_j exceeds the threshold $y_{th} = 1.6$. This choice ensures that only marked variations of the oscillator trajectory are counted as firing events. Consistently with the analysis of experimental recordings (see Sec. II B), we set the time bin t_b equal to the inter spike interval. Note that in the model t_b is a non-dimensional constant, its mapping to a physical time value must therefore be calibrated against experimental data (Sec. III B).

2. Active Kuramoto model with Inhibition Dynamics

To take into account a second population of oscillators representing inhibitory neurons, we have extended the dynamics of Eq. (6). In the purely excitatory model, the interaction term tends to align the phase θ_j of each neuron to the average phase of the population Ψ , defined through the following relation

$$R e^{i\Psi} = \frac{1}{N} \sum_{j=1}^N e^{i\theta_j}, \quad (8)$$

where R is the norm of the Kuramoto-Daido order parameters [36]. Accordingly, Eq. (6) can be rewritten in terms of R and Ψ as

$$\dot{\theta}_j = \omega_j + \xi_j - KR \sin(\theta_j - \Psi) + a \sin(\theta_j) \quad (9)$$

which makes the mean-field alignment nature of the interaction explicit [10, 16, 35, 36]. Many theoretical and numerical studies have generalized Eq. (9) to multi-population systems [10, 12, 16, 19, 34, 36]. In such models, the interactions between different populations have the same form as in Eq. (9), but with distinct coupling constants K , which may also take negative values. While this assumption is reasonable for excitatory neurons, it is not biologically appropriate for an inhibitory population. Indeed, when an inhibitory neuron fires, the total activity of the network must decrease. Conversely, it has been shown that this type of inhibition interaction might enhance activity and synchronization [19, 20]. This unrealistic scenario occurs because inhibition is modeled as a

purely repulsive force, which may induce excitatory neurons to spike when the inhibitory oscillators' phase is close to the stable position of the excitatory ones.

To heal the contradiction with the behavior of real neurons, we have modified the conservative potential so that

$$\begin{aligned}\dot{\theta}_j^E &= \omega_j + \xi_j - K_E R_E \sin(\theta_j^E - \Psi_E) + [a + K_I R_I^2 \cos^2(\Psi_I)] \sin(\theta_j^E) \\ \dot{\theta}_j^I &= \omega_j + \xi_j - K_E R_E \sin(\theta_j^I - \Psi_E) + [a + K_I R_I^2 \cos^2(\Psi_I)] \sin(\theta_j^I)\end{aligned}\quad (10)$$

where R_E , R_I , Ψ_E and Ψ_I are defined by

$$\begin{aligned}R_E e^{i\Psi_E} &= \frac{1}{N_E} \sum_{j=1}^{N_E} e^{i\theta_j^E}, \\ R_I e^{i\Psi_I} &= \frac{1}{N_I} \sum_{j=1}^{N_I} e^{i\theta_j^I}.\end{aligned}\quad (11)$$

In Eq. (10), each neuron tends to align its phase with the average activity of the excitatory population, while inhibitory activity modulates the conservative potential. This is implemented by the terms in square brackets, which effectively drive all neurons towards their quiescent state depending on the average activity of inhibitory neurons, reducing their firing probability.

By setting $K_E = K \frac{N_E}{N}$ and $K_I = K \frac{N_I}{N}$, the model reduces to Eq. (9) when $N_E = N$. From the biological point of view, the inhibition dynamics implemented here captures the regulatory effect of inhibition in balancing excitation. In different models [6, 14], this stabilization is introduced by synaptic resource depletion only, but here we focus exclusively on inhibition dynamics and do not include explicitly the synaptic fatigue. The phase diagram of this model as a function of the amplitude of noise σ_ξ and the amplitude of the conservative potential a (not shown here) closely resembles the one already obtained for the purely excitatory case in [7]. The parameters have been set as follows: $K = 1$, $\bar{\omega} = 1$, $\sigma_\omega = 0.05$, $a = 0.92$, $\sigma_\xi = 0.35$, and $N = 750$. To determine the avalanche dynamics in this case, we apply the same procedure described above for the single-population model.

3. External Poisson noise

The variability among different experimental samples within a given network class (i.e., 100E or 75E:25I) not only leads to different scaling exponents but can also be quantified by examining the Fano Factor, that is the ratio between the variance and the mean of the number of spikes within a given time window. For the purely excitatory networks, there is a positive correlation between the exponents and this measure of variability (see SM [37]). Conversely, for the 75E:25I networks, the measures of

its amplitude depends on the activity of the inhibitory population. Defining the phases of a generic excitatory or inhibitory neuron as $\theta_j^{(E)}$ and $\theta_j^{(I)}$, their evolution equations are:

this ratio are too noisy to reliably assess the variability. To reproduce this variability in numerical simulations, we have included an additional noise source into the model. Noise is treated as an external contribution superposed to the simulated raster plot. In particular, in each channel and to each bin we have added an entry that has probability p of being active and probability $1 - p$ of being inactive. The external noise has a double effect. On one side, it reduces the probability of small avalanches by merging avalanches together. On the other hand, it reduces the inter-spike time, and therefore the time-bin t_b , used for the avalanche detection, fragmenting large avalanches into smaller ones. In both single- and two-population models, two different noise levels have been used ($p = 10^{-5}$ and $p = 10^{-4}$ for 100E, $p = 10^{-4}$ and $p = 5 \cdot 10^{-4}$ for 75E:25I).

H. Power-law fitting and error estimation

Power-law exponents for avalanche size, duration, and inter-event interval distributions have been estimated using least-squares fitting in log-log scale. Empirical distributions have been first log-binned to reduce fluctuations in the tails. Linear regression has been then applied on the log-binned probability density function. Fitting has been restricted to the scaling regime, namely selected linear regions of the log-log plots, excluding the peak associated with synchronized bursting and the noisy tail at large event sizes. To assess the robustness of the fitted exponents, we have systematically varied the fitting window. The reported uncertainty has been taken as half the maximum variation observed across the tested ranges. This approach reflects how sensitive the fitted exponent is to the selected bounds and provides a conservative estimate of the exponents in data with non-ideal power-law. Maximum likelihood methods and goodness-of-fit tests have not been applied, because bimodality violates their assumptions. The error on derived quantities, as the exponent γ estimated by Eq. (3), has been computed using the standard error propagation formula. The error on crossover time estimated from the distribution of inter-times $P(\Delta t)$ has been computed from the intersection between the two power-laws by varying the fitting

window. The difference of conditional probabilities δP , instead, has been computed as an average over $M = 10^3$ surrogate distributions while the error bars have been estimated as 3 standard deviations of the Gaussian distribution obtained for reshuffled data. Finally, the crossover time for δP has been estimated from the plots. An uncertainty of $5t_b$ has been assigned, reflecting the variability in identifying the crossover curve.

III. RESULTS

A. Avalanches

We investigate the properties of neuronal avalanches in electrophysiological recordings of hiPSC-derived cortical cultures with different excitatory/inhibitory (E/I) ratios: purely excitatory (100E) and physiological (75E:25I) networks. The avalanche size and duration distributions (Fig. 2 (a), (b), (e), (f)), exhibit bimodal shapes. In particular, large and long-lasting avalanches associated with network-level synchronization phenomena show narrow distributions, while avalanches of intermediate size follow a power-law pattern extending for nearly two decades. Analysis of individual samples (Tab. II) reveals that both 100E and 75E:25I networks can be divided into two subgroups based on their scaling exponent values for avalanche size and duration distributions. Average group distributions indicate the existence of an intermediate scaling regime with exponents τ and α which are larger for higher values of the Fano factor (see SM [37]).

Interestingly, the decrease of the distributions is steeper for fully excitatory networks compared to physiological ones. These results can be explained in terms of the experimental observation [21], evidencing that in fully excitatory networks synchronization occurs with a higher frequency with respect to physiological cultures. Therefore, synchronization hampers the occurrence of large avalanches in favour of bursts encompassing the entire system.

Sample	100E		75E:25I	
	τ	α	τ	α
1	3.3 ± 0.2	3.6 ± 0.3	2.9 ± 0.2	3.4 ± 0.2
2	2.8 ± 0.1	3.2 ± 0.2	3.0 ± 0.2	3.3 ± 0.3
3	2.8 ± 0.1	3.3 ± 0.2	2.1 ± 0.1	2.5 ± 0.2
4	3.3 ± 0.2	3.7 ± 0.3	2.0 ± 0.1	2.6 ± 0.2
5	3.2 ± 0.2	3.6 ± 0.3	2.0 ± 0.2	2.4 ± 0.2
6	3.2 ± 0.2	3.5 ± 0.3	–	–

TABLE II. Critical exponents of the avalanche distributions for individual samples for the experiments on purely excitatory (100E) and physiological (75E:25I) networks.

Notably, the exponents τ and α reported in Tab. III, are larger than those usually found in literature for spontaneous activity in neuronal cultures and not compatible with those of the universality class of the mean-field branching process ($\tau = \frac{3}{2}$ and $\alpha = 2$) [1, 3, 38]. An

emerging paradigm in brain dynamics is the concept of self-organized bistability [14], which suggests that neural networks operate near a synchronization transition, where scale-free avalanches can arise [6, 7, 14]. To explore this, we employ the active rotator model generalizing the Kuramoto oscillators introducing an excitable behavior [12, 13]. This excitability drives the system activity to organize into avalanches whose size and duration distributions exhibit bimodality, consisting of a power-law regime followed by a bump associated with synchronized bursting [7, 14]. We extend the active Kuramoto model in two ways (see Sec. II G). First, we incorporate an external noise to reproduce the experimental variability of exponents. Second, we develop a two-population version of the model to account explicitly for the effects of the inhibitory population through a biological grounded modulation of the conservative potential. As shown in Fig. 2, both the single- and two-population models correctly reproduce the bimodal distributions observed experimentally: an initial power law regime followed by a bump at large S and T corresponding to synchronization phenomena. Moreover, tuning the external noise allows reproducing the variability in exponent values (Tab. III).

To further investigate the power-law activity regimes, we also analyze the behavior of the average size of avalanches conditioned on the duration T , $\langle S \rangle_{S|T}$, and compare the results of experimental and simulated data (Fig. 3). The relation between $\langle S \rangle_{S|T}$ and T deviates from the power law behavior when the bursts at large S and T are approached, in agreement with the Sethna theory holding only at the critical point, here in the scaling regime.

Data	τ	α	γ	γ (Eq. (3))
Exp 100E	2.7 ± 0.2	3.3 ± 0.2	1.3 ± 0.1	1.3 ± 0.2
$p = 10^{-5}$ 100E	2.8 ± 0.2	3.3 ± 0.2	1.2 ± 0.1	1.3 ± 0.2
Exp 100E	3.1 ± 0.2	3.7 ± 0.3	1.2 ± 0.1	1.3 ± 0.2
$p = 10^{-4}$ 100E	3.1 ± 0.3	3.7 ± 0.2	1.2 ± 0.1	1.3 ± 0.2
Exp 75E:25I	2.1 ± 0.2	2.5 ± 0.2	1.2 ± 0.1	1.3 ± 0.3
$p = 10^{-4}$ 75E:25I	2.1 ± 0.3	2.5 ± 0.2	1.3 ± 0.2	1.3 ± 0.3
Exp 75E:25I	2.9 ± 0.2	3.3 ± 0.2	1.2 ± 0.1	1.2 ± 0.2
$p = 5 \cdot 10^{-4}$ 75E:25I	2.7 ± 0.3	3.1 ± 0.2	1.3 ± 0.2	1.2 ± 0.3

TABLE III. Exponents of size (τ) and duration (α) distributions and of conditional expectation $\langle S \rangle_{S|T}$ (γ) for different data-sets. Except for the last column, where the scaling relation (3) has been used, the values refer to results obtained from a fitting procedure (see Sec. II).

Moreover, for both experimental and numerical networks, the exponent γ shows minimal variations between purely excitatory and physiological networks (Figs. 3). These considerations further support our hypothesis that differences between groups within the same experimental setup are akin to some form of noise. As explained above, the effect of the noise mostly results in larger exponents. Interestingly, the values of γ determined by the fitting procedure are coherent with those estimated from the scaling relation (3). Moreover, those values are com-

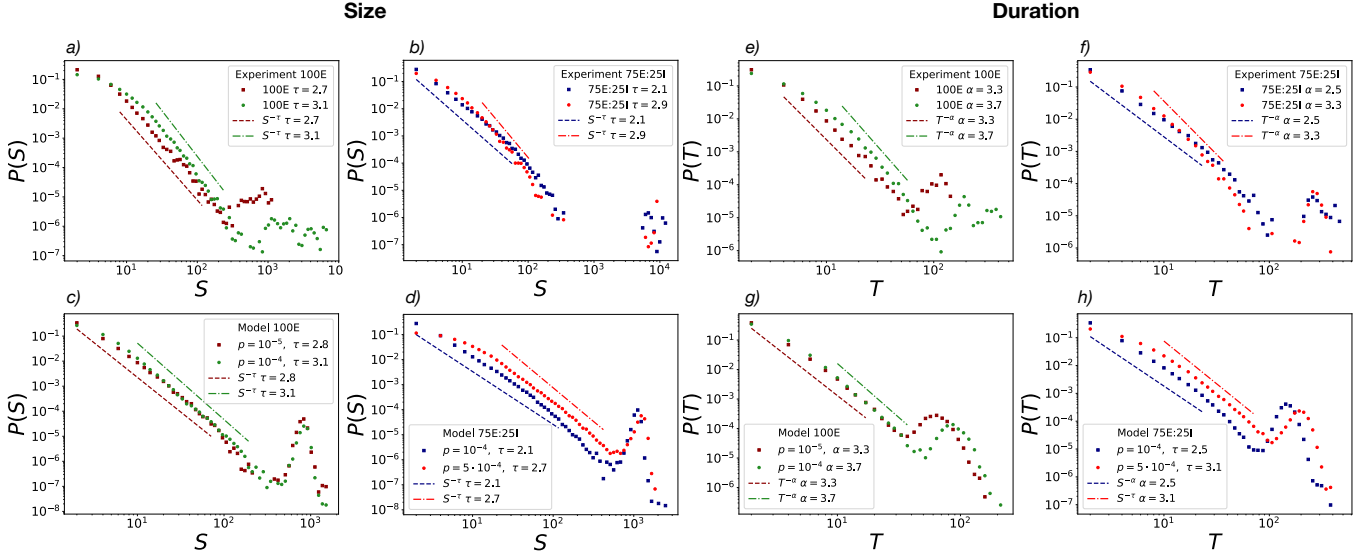


FIG. 2. Size and duration distributions for experimental and numerical data with superimposed theoretical power-law behavior (dashed and dot-dashed lines). Circles and squares represent samples with high or low values of the exponents τ and α , respectively. a) Size distribution of experiments on purely excitatory networks. b) Size distribution of experiments on physiological networks. c-d) Size distributions of single- and two- population active Kuramoto model with inhibition dynamics. e) Duration distribution of experiments on purely excitatory networks. f) Duration distribution of experiments on physiological networks. g-h) Duration distributions of single- and two- population active Kuramoto model with inhibition dynamics.

patible with those reported in [31].

B. Inter-times

To probe the temporal correlations of activity, we measure the distribution of inter-times Δt between successive avalanches. This distribution is able to discriminate between a Poisson process, in which case it exhibits an exponential behavior, and a process with temporal correlations if a power-law behavior is detected. Assuming that small-size avalanches are mostly dominated by external noise, we restrict our analysis to sizes exceeding a given threshold S^* , as in [39]. We consider two values of the threshold per network type, corresponding to the two subgroups identified earlier. The experimental inter-event interval distributions, in units of t_b and averaged over the samples of each subgroup, exhibit a clear crossover between two power-law regimes (Fig. 4 (a-b-e-f)). Importantly, the corresponding distributions $P(\Delta t)$ for both single- and two-population models closely match the experimental findings, including the crossover between the two power-law regimes (Fig. 4 (c-d-g-h)). Therefore, for both experimental and numerical data, the distributions indicate the presence of complex temporal correlations resulting in the crossover (Fig. 4). The two exponents $\mu_<$ (for small Δt) and $\mu_>$ (for large Δt) are consistent from sample to sample (Tabs. IV-V), since size thresholding reduces the effect of external noise.

To better quantify temporal correlations, we estimate the crossover time \mathcal{T}_I in ms for each sample (Tab. VI).

Sample	100E			75E:25I		
	$\mu_<$	$\mu_>$	S^*	$\mu_<$	$\mu_>$	S^*
1	1.1 ± 0.3	1.9 ± 0.2	5	0.9 ± 0.2	2.0 ± 0.3	9
2	1.1 ± 0.2	2.0 ± 0.3	4	0.9 ± 0.2	1.9 ± 0.2	9
3	1.0 ± 0.2	2.0 ± 0.3	4	1.2 ± 0.2	2.0 ± 0.3	8
4	1.1 ± 0.3	2.3 ± 0.3	5	1.1 ± 0.2	1.9 ± 0.2	8
5	1.2 ± 0.3	2.3 ± 0.4	5	1.1 ± 0.2	2.0 ± 0.2	8
6	1.1 ± 0.2	2.4 ± 0.4	5	—	—	—

TABLE IV. Inter-time distribution exponents $\mu_<$ and $\mu_>$ resulting from the analysis of individual samples for experiments on purely excitatory (100E) and physiological (75E:25I) networks.

Data	$\mu_<$	$\mu_>$
Exp 100E	1.1 ± 0.2	2.0 ± 0.3
$p = 10^{-5}$ 100E	1.1 ± 0.2	2.3 ± 0.3
Exp 100E	1.2 ± 0.2	2.3 ± 0.2
$p = 10^{-4}$ 100E	0.9 ± 0.2	1.9 ± 0.3
Exp 75E25I	1.2 ± 0.1	1.9 ± 0.2
$p = 10^{-4}$ 75E25I	1.2 ± 0.2	1.9 ± 0.3
Exp 75E25I	0.9 ± 0.1	1.9 ± 0.2
$p = 5 \cdot 10^{-4}$ 75E25I	1.0 ± 0.2	2.3 ± 0.3

TABLE V. Exponents $\mu_<$ and $\mu_>$ of the average inter-time distribution.

Purely excitatory networks exhibit shorter \mathcal{T}_I than physiological ones, consistent with oscillations in the alpha band.

To compare these results with numerical simulations, a physical timescale must be assigned to the model.

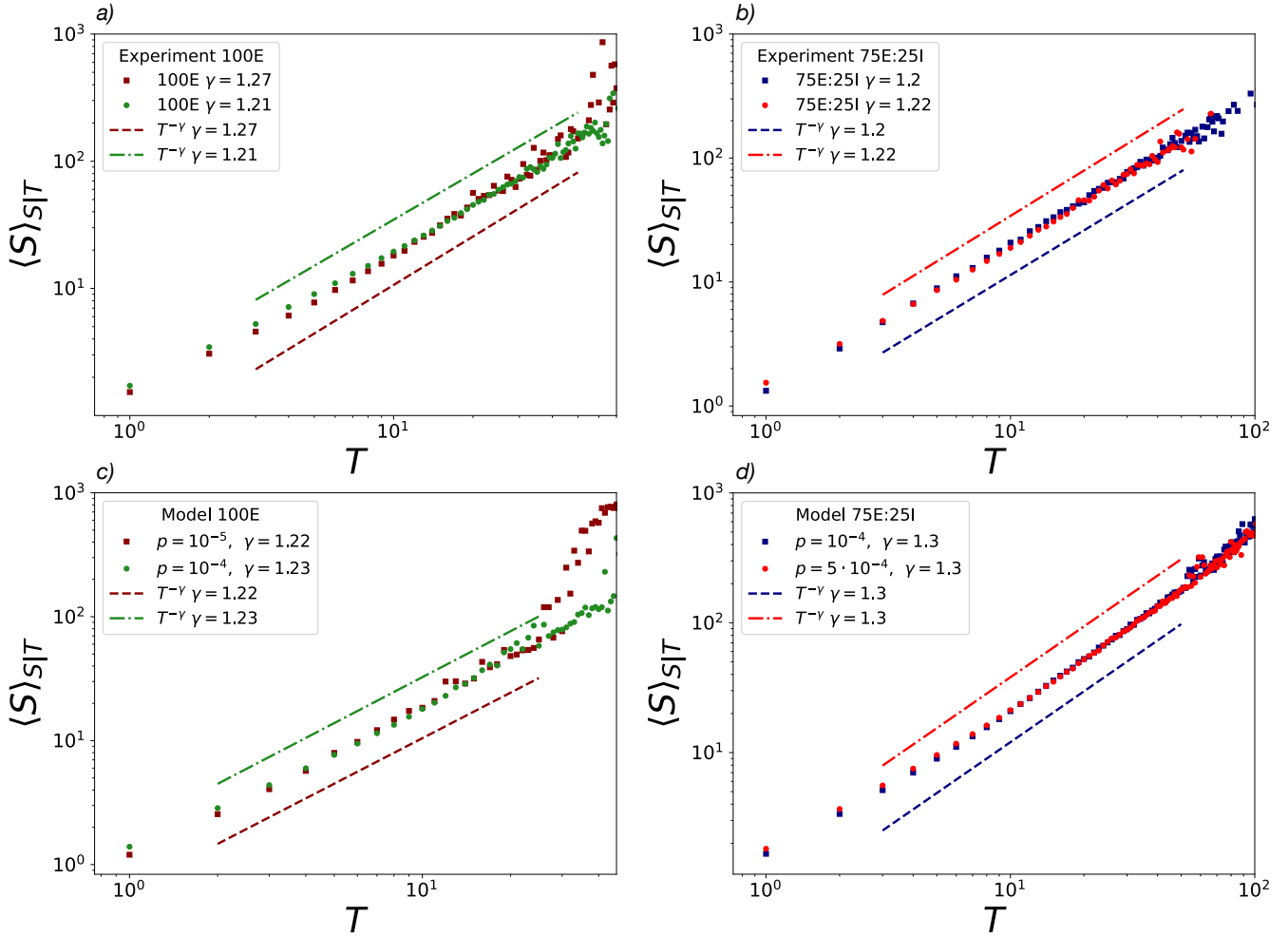


FIG. 3. Conditional expectation of avalanche size $\langle S \rangle_{S|T}$ for experimental and numerical data with superimposed theoretical power-law behavior (dashed and dot-dashed lines). Circles and squares represent groups with high or low values of the exponents τ and α , respectively. a) Experiments on purely excitatory networks. b) Experiments on physiological networks. c-d) Single- and two- population active Kuramoto model with inhibition dynamics.

Sample	100E		75E:25I	
	\mathcal{T}_I (ms)	\mathcal{T}_C (ms)	\mathcal{T}_I (ms)	\mathcal{T}_C (ms)
1	90 ± 50	80 ± 40	200 ± 70	180 ± 60
2	130 ± 90	110 ± 60	110 ± 30	90 ± 30
3	140 ± 80	100 ± 50	230 ± 30	170 ± 60
4	100 ± 50	90 ± 50	100 ± 60	120 ± 40
5	40 ± 30	40 ± 20	130 ± 50	100 ± 50
6	30 ± 10	30 ± 20	–	–

TABLE VI. Crossover time of the inter-time distributions \mathcal{T}_I and of the conditional probability differences \mathcal{T}_C for individual samples for the experiments on purely excitatory (100E) and physiological networks (75E:25I).

Our choice is to match the time-bin of the model to the average experimental time-bin, where the average is performed over the respective subgroups (more details in SM [37]). Thus, it is possible to express the crossover time \mathcal{T}_I in ms. The average experimental

Data	\mathcal{T}_I (ms)	\mathcal{T}_C (ms)
Exp 100E	135 ± 60	105 ± 40
$p = 10^{-5}$ 100E	145 ± 80	75 ± 30
Exp 100E	65 ± 20	60 ± 20
$p = 10^{-4}$ 100E	125 ± 50	60 ± 20
Exp 75E25I	155 ± 30	130 ± 30
$p = 10^{-4}$ 75E25I	125 ± 90	75 ± 30
Exp 75E25I	155 ± 40	135 ± 40
$p = 5 \cdot 10^{-4}$ 75E25I	175 ± 70	70 ± 30

TABLE VII. Comparison between the average crossover times extrapolated from the inter-time distributions \mathcal{T}_I and from the conditional probability differences \mathcal{T}_C for experimental and numerical data. The adimensional crossover times for numerical data are 14 ± 8 and 19 ± 7 (100E) and 13 ± 10 and 19 ± 8 (75E:25I) for the low and high noise cases, respectively.

crossover-times \mathcal{T}_I and the corresponding values computed from simulations are reported in Tab. VII. All

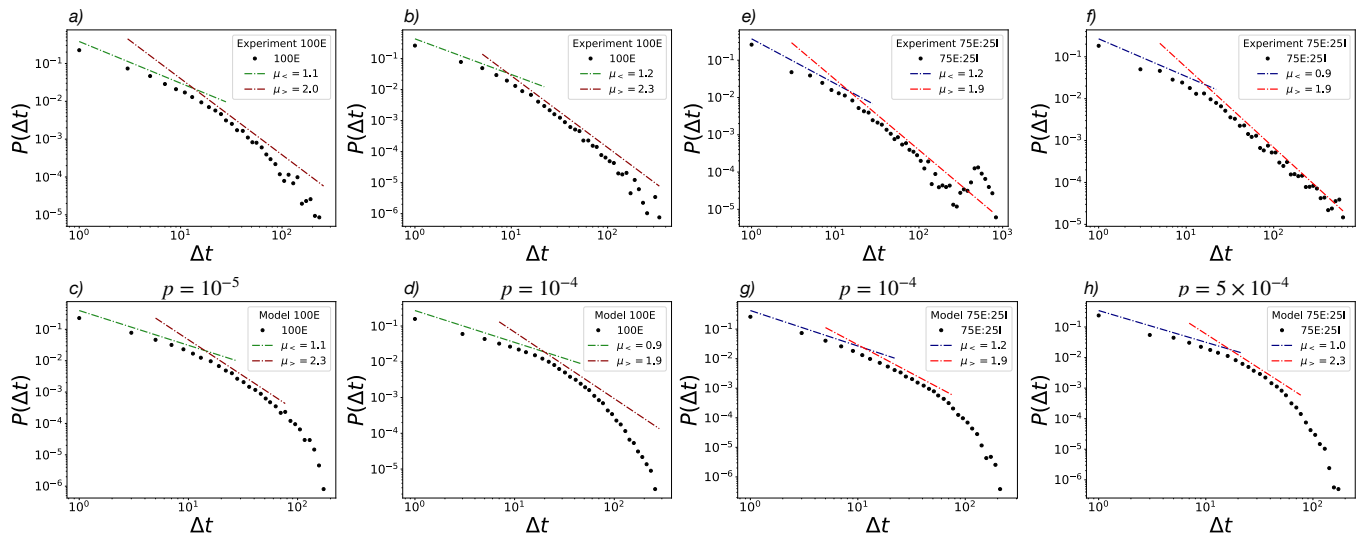


FIG. 4. Inter-time distributions with superimposed theoretical power-law behavior. The crossover time can be estimated from the intersection between the two power-law regimes. a-b) Experiments on purely excitatory networks. e-f) Experiments on physiological networks. c-d-g-h) Single- and two- population active Kuramoto model with inhibition dynamics.

model-derived crossover-times \mathcal{T}_I , except for the purely excitatory model with $p = 10^{-4}$, are compatible with their experimental counterparts. The discrepancy observed for the 100E case is probably related to an overestimation of the average time-bin t_b of the corresponding experiment (see SM [37]).

C. Correlation between avalanche size and occurrence time

Finally, we investigate the correlations between successive avalanches by analyzing the conditional probability $P(s_0, t_0)$ to observe two consecutive avalanches with a size difference $\Delta S = S^{(i+1)} - S^{(i)} \leq s_0$ given the value of their inter-time $\Delta t \leq t_0$. More specifically, we consider the difference between conditional probabilities

$$\delta P(s_0, t_0) = P(s_0, t_0) - \bar{P}(s_0, t_0) \quad (12)$$

where $P(s_0, t_0)$ and $\bar{P}(s_0, t_0)$ are the conditional probabilities computed on the original or reshuffled avalanche sequence, respectively (see Sec. II). A careful analysis of this quantity can reveal correlations between differences in avalanche size and corresponding quiescent times [22, 23, 33, 38]. In all experimental samples the quantity δP exhibits a complex scenario (see SM [37]). In Fig. 5 (a-b-e-f), the average curves for each subgroup networks clearly display a crossover between different regimes, also reproduced by the Kuramoto models (Fig. 5 c-d-g-h). For small values of t_0 , δP presents a positive maximum for $s_0 < 0$ and a negative minimum for $s_0 > 0$, indicating that for avalanches close in time, i.e. occurring after a short quiescence period, the second avalanche tends to be smaller than the preceding one (attenuation

regime). For large values of t_0 , δP has the opposite behavior with its maximum at positive values of s_0 , implying that for avalanches distant in time, the second avalanche tends to be larger than the preceding one (amplification regime). By varying t_0 , δP changes continuously between the two different regimes, becoming almost flat at a particular value of t_0 , identifying the crossover time \mathcal{T}_C between the attenuation and amplification dynamics.

For each individual sample, we estimate the crossover time \mathcal{T}_C and we report the results in Tab. VI. We notice that \mathcal{T}_C is smaller for purely excitatory networks than physiological ones. Moreover, \mathcal{T}_I obtained from the inter-time distributions and \mathcal{T}_C from the crossover of conditional probability differences are comparable within the error bars. Let us also stress that the same kind of observations can be made for numerical data, as can be seen in Tabs. VII.

IV. DISCUSSION

Our results demonstrate that hiPSC-derived neuronal networks display the coexistence of scale free avalanches with strongly synchronized bursts, and that these features are reproduced by our novel Kuramoto model. Taken together, the experiments and theory support the view that neuronal systems operate in a regime of self-organized bistability, at the boundary of synchronization where power-law avalanche regimes and oscillatory events naturally emerge [6, 7]. This behavior differs from what already found in in vitro models of cortical murine networks: in the seminal works in acute cortical slices [1] and some years later in dissociated cortical

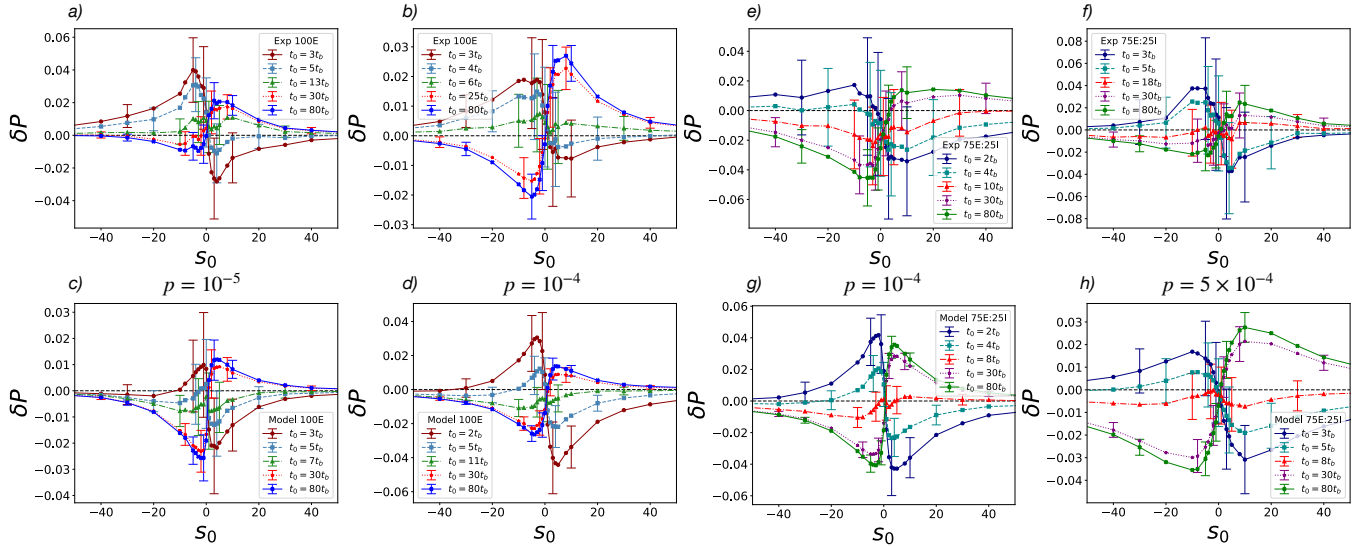


FIG. 5. Difference δP between conditional probabilities of observing a difference between subsequent avalanche sizes smaller than a given value s_0 conditioned on the fact that their inter-time is lower than t_0 . The crossover time can be estimated as the time when the switching between amplification and attenuation regime occurs. a-b) Experiments on purely excitatory networks. e-f) Experiments on physiological networks. c-d-g-h) Single- and two- population active Kuramoto model with inhibition dynamics.

cultures [2], a power-law behavior in the avalanches' distributions of size and lifetime was found. The presence of a bump of activity in correspondence of big avalanches was achieved in such experimental models by altering the excitatory/inhibitory balance of the networks with the administration of GABA antagonists like bicuculline or picrotoxin. In the recordings analyzed in this work, where neurons derive from hiPSCs, the bistable dynamics (although with different exponents) persists in both physiological (75E:25I) and fully excitatory networks (100E). This evidence could be explained by speculating a peculiar network connectivity for hiPSCs derived neuronal networks: as computational studies proved [40, 41] the complexity of the network organization pushes the network dynamics towards power-law and/or bistable dynamics: Massobrio, et al. simulated a power law regime only with a network connectivity organized with the existence of hubs and clusters of neurons. This feature cannot be explained by the computational choice pursued in this work: the Kuramoto model implements a full connectivity matrix, thus ignoring possible connectivity rules.

The central innovation of this work is the explicit incorporation of inhibition dynamics into the Kuramoto framework. Previous oscillator models successfully capture synchronization phenomena [17, 19] but represent inhibition in a manner that results in a non-biological enhancement of activity [20]. Here, instead, we implement the inhibition dynamics by letting the amplitude of the conservative potential be dependent on the inhibitory activity, establishing a biologically grounded mechanism of regulation that accounts for the coexistence of avalanche-dominated and synchronized states. We also found that

an external Poisson noise reproduces the variability observed across experimental samples. This result is consistent with previous reports showing that apparent critical scaling might emerge from stochastic variability [28–30] and that noise actively modulates avalanche dynamics [22].

As discussed in Sec. III A, the exponents τ and α characterizing the avalanche size and duration distributions, measured in both experiments and simulations, differ from those predicted by the mean-field branching process. Consequently, the scaling exponent γ also deviates from its theoretical value $\gamma = 2$. Previous studies [42] have attributed such discrepancies to subsampling effects in experimental recordings. While this explanation may account for the experimental data, it does not explain the behavior of our model. Moreover, the values of γ estimated in Sec. III A are consistent with those reported in [31], where the exponents τ and α likewise differ from the mean-field predictions. Beyond static avalanche statistics [1–3, 38], the analysis of inter-time distributions and conditional probabilities has unveiled temporal correlations between consecutive avalanches. The inter-time distributions exhibited a crossover between two different power-law regimes. This feature has already been observed in human brain, where the crossover is related to the α rhythm [23]. Interestingly, also in our study this crossover falls into the alpha-band for both purely excitatory and physiological networks. The analysis of conditional probabilities further confirms the existence of a crossover between attenuation and amplification regimes, with a characteristic time-scale that closely matches the crossover-time estimated from the inter-event time distributions, as expected [23]. The ability of the model to

reproduce not only the synchronized activity but also the avalanche dynamics, including these memory-like effects strongly suggests self-organized bistability as a unifying paradigm for brain dynamics, linking avalanche propagation, synchronization, and temporal correlations within a single theoretical construct.

ACKNOWLEDGMENTS

The authors acknowledge funding from NEXTGENERATIONEU (NGEU) funded by the Ministry of

University and Research (MUR), National Recovery and Resilience Plan (NRRP), and Project MNESYS (PE0000006)-A multiscale integrated approach to the study of the nervous system in health and disease (DN. 1553 11.10.2022). AS acknowledges funding from the Italian Ministero dell'Università e della Ricerca under the programme PRIN 2022 ("re-ranking of the final lists"), number 2022KWTEB7, cup B53C24006470006.

-
- [1] J. M. Beggs and D. Plenz, Neuronal avalanches in neocortical circuits, *The Journal of Neuroscience* **23**, 11167–11177 (2003).
- [2] V. Pasquale, P. Massobrio, L. Bologna, M. Chiappalone, and S. Martinoia, Self-organization and neuronal avalanches in networks of dissociated cortical neurons, *Neuroscience* **153**, 1354–1369 (2008).
- [3] J. M. Beggs and N. Timme, Being critical of criticality in the brain, *Frontiers in Physiology* **3**, 10.3389/fphys.2012.00163 (2012).
- [4] M. Gutnick, B. Wolfson, and F. Baldino Jr, Synchronized neuronal activities in neocortical explant cultures, *Experimental brain research* **76**, 131 (1989).
- [5] S. di Santo, R. Burioni, A. Vezzani, and M. A. Muñoz, Self-organized bistability associated with first-order phase transitions, *Phys. Rev. Lett.* **116**, 240601 (2016).
- [6] S. di Santo, P. Villegas, R. Burioni, and M. A. Muñoz, Landau–ginzburg theory of cortex dynamics: Scale-free avalanches emerge at the edge of synchronization, *Proceedings of the National Academy of Sciences* **115**, 10.1073/pnas.1712989115 (2018).
- [7] V. Buendía, P. Villegas, R. Burioni, and M. A. Muñoz, Hybrid-type synchronization transitions: Where incipient oscillations, scale-free avalanches, and bistability live together, *Physical Review Research* **3**, 023224 (2021).
- [8] V. Buendía, P. Villegas, R. Burioni, and M. A. Muñoz, The broad edge of synchronization: Griffiths effects and collective phenomena in brain networks, *Philosophical Transactions of the Royal Society A: Mathematical, Physical and Engineering Sciences* **380**, 10.1098/rsta.2020.0424 (2022).
- [9] Y. Kuramoto, International symposium on mathematical problems in theoretical physics, *Lecture notes in Physics* **30**, 420 (1975).
- [10] J. A. Acebrón, L. L. Bonilla, C. J. Pérez Vicente, F. Ritort, and R. Spigler, The kuramoto model: A simple paradigm for synchronization phenomena, *Reviews of modern physics* **77**, 137 (2005).
- [11] S. Shinomoto and Y. Kuramoto, Phase transitions in active rotator systems, *Progress of Theoretical Physics* **75**, 1105 (1986).
- [12] H. Sakaguchi and Y. Kuramoto, A soluble active rotator model showing phase transitions via mutual entertainment, *Progress of Theoretical Physics* **76**, 576 (1986).
- [13] H. Sakaguchi, S. Shinomoto, and Y. Kuramoto, Phase transitions and their bifurcation analysis in a large population of active rotators with mean-field coupling, *Progress of Theoretical Physics* **79**, 600 (1988).
- [14] V. Buendía, S. di Santo, P. Villegas, R. Burioni, and M. A. Muñoz, Self-organized bistability and its possible relevance for brain dynamics, *Phys. Rev. Res.* **2**, 013318 (2020).
- [15] G. Ódor, I. Papp, S. Deng, and J. Kelling, Synchronization transitions on connectome graphs with external force, *Frontiers in Physics* **11**, 10.3389/fphy.2023.1150246 (2023).
- [16] S. Shinomoto and Y. Kuramoto, Cooperative phenomena in two-dimensional active rotator systems, *Progress of theoretical physics* **75**, 1319 (1986).
- [17] E. Montbrió, J. Kurths, and B. Blasius, Synchronization of two interacting populations of oscillators, *Physical Review E—Statistical, Nonlinear, and Soft Matter Physics* **70**, 056125 (2004).
- [18] E. Montbrió, D. Pazó, and A. Roxin, Macroscopic description for networks of spiking neurons, *Physical Review X* **5**, 021028 (2015).
- [19] E. Montbrió and D. Pazó, Kuramoto model for excitation-inhibition-based oscillations, *Physical Review Letters* **120**, 10.1103/physrevlett.120.244101 (2018).
- [20] T. Shimokawa and S. Shinomoto, Inhibitory neurons can facilitate rhythmic activity in a neural network, *Physical Review E* **73**, 10.1103/physreve.73.066221 (2006).
- [21] G. Parodi, M. Brofiga, V. P. Pastore, M. Chiappalone, and S. Martinoia, Deepening the role of excitation/inhibition balance in human ipscs-derived neuronal networks coupled to meas during long-term development, *Journal of Neural Engineering* **20**, 056011 (2023).
- [22] F. Lombardi, H. J. Herrmann, D. Plenz, and L. de Arcangelis, Temporal correlations in neuronal avalanche occurrence, *Scientific Reports* **6**, 10.1038/srep24690 (2016).
- [23] F. Lombardi, H. J. Herrmann, L. Parrino, D. Plenz, S. Scarpetta, A. E. Vaudano, L. De Arcangelis, and O. Shriki, Beyond pulsed inhibition: Alpha oscillations modulate attenuation and amplification of neural activity in the awake resting state, *Cell reports* **42** (2023).
- [24] K. Dahmen and J. P. Sethna, Hysteresis, avalanches, and disorder-induced critical scaling: A renormalization-group approach, *Physical Review B* **53**, 14872 (1996).
- [25] O. Perković, K. Dahmen, and J. P. Sethna, Avalanches, barkhausen noise, and plain old criticality, *Physical review letters* **75**, 4528 (1995).

- [26] M. C. Kuntz and J. P. Sethna, Noise in disordered systems: The power spectrum and dynamic exponents in avalanche models, *Physical Review B* **62**, 11699–11708 (2000).
- [27] A. Maccione, M. Gandolfo, P. Massobrio, A. Novellino, S. Martinoia, and M. Chiappalone, A novel algorithm for precise identification of spikes in extracellularly recorded neuronal signals, *Journal of Neuroscience Methods* **177**, 241–249 (2009).
- [28] J. Touboul and A. Destexhe, Can power-law scaling and neuronal avalanches arise from stochastic dynamics?, *PLoS ONE* **5**, e8982 (2010).
- [29] J. Touboul and A. Destexhe, Power-law statistics and universal scaling in the absence of criticality, *Physical Review E* **95**, 10.1103/physreve.95.012413 (2017).
- [30] V. Priesemann and O. Shriki, Can a time varying external drive give rise to apparent criticality in neural systems?, *PLOS Computational Biology* **14**, e1006081 (2018).
- [31] A. J. Fontenele, N. A. de Vasconcelos, T. Feliciano, L. A. Aguiar, C. Soares-Cunha, B. Coimbra, L. Dalla Porta, S. Ribeiro, A. J. Rodrigues, N. Sousa, P. V. Carelli, and M. Copelli, Criticality between cortical states, *Physical Review Letters* **122**, 10.1103/physrevlett.122.208101 (2019).
- [32] F. Lombardi, H. J. Herrmann, C. Perrone-Capano, D. Plenz, and L. de Arcangelis, Balance between excitation and inhibition controls the temporal organization of neuronal avalanches, *Phys. Rev. Lett.* **108**, 228703 (2012).
- [33] L. de Arcangelis, C. Godano, J. R. Grasso, and E. Lipiello, Statistical physics approach to earthquake occurrence and forecasting, *Physics Reports* **628**, 1 (2016).
- [34] A. T. Winfree, *The geometry of biological time*, Vol. 2 (Springer, 1980).
- [35] Y. Kuramoto, Collective synchronization of pulse-coupled oscillators and excitable units, *Physica D: Nonlinear Phenomena* **50**, 15 (1991).
- [36] S. H. Strogatz, From kuramoto to crawford: exploring the onset of synchronization in populations of coupled oscillators, *Physica D: Nonlinear Phenomena* **143**, 1 (2000).
- [37] Supplementary material, [URL_will_be_inserted_by_publisher](#).
- [38] L. de Arcangelis, F. Lombardi, and H. J. Herrmann, Criticality in the brain, *Journal of Statistical Mechanics: Theory and Experiment* **2014**, P03026 (2014).
- [39] F. Bianchi, M. Thielmann, L. De Arcangelis, and H. J. Herrmann, Critical bursts in filtration, *Physical review letters* **120**, 034503 (2018).
- [40] S. Pajevic and D. Plenz, Efficient network reconstruction from dynamical cascades identifies small-world topology of neuronal avalanches, *PLoS computational biology* **5**, e1000271 (2009).
- [41] P. Massobrio, V. Pasquale, and S. Martinoia, Self-organized criticality in cortical assemblies occurs in concurrent scale-free and small-world networks, *Scientific reports* **5**, 10578 (2015).
- [42] J. P. Neto, F. P. Spitzner, and V. Priesemann, Sampling effects and measurement overlap can bias the inference of neuronal avalanches, *PLOS Computational Biology* **18**, e1010678 (2022).